Chemical Science

Cite this: *Chem. Sci.*, 2012, **3**, 2158

www.rsc.org/chemicalscience

EDGE ARTICLE

Supramolecular architectures for controlling slow magnetic relaxation in field-induced single-molecule magnets†

Fatemah Habib,[a] Jérôme Long,[a] Po-Heng Lin,[a] Ilia Korobkov,[a] Liviu Ungur,[c] Wolfgang Wernsdorfer,[d] Liviu F. Chibotaru[c] and Muralee Murugesu*[ab]

Received 7th December 2011, Accepted 18th March 2012
DOI: 10.1039/c2sc01029a

In order for molecular magnetic materials to become functional, they must retain their magnetization at reasonable temperatures implying high energy barriers for spin reversal. The field of single-molecule magnets (SMMs) has recently experienced an explosion of research targeting these high anisotropic barriers. Achieving such feats has involved increasing the spin of a complex and/or increasing the inherent magnetic anisotropy. Exerting control over the total spin of a complex has been possible contrary to controlling the global anisotropy. Herein, we report the experimental and theoretical study of local anisotropy alignment on Dy^{III} metal centers and their orientation relative to other centers in rare, dinuclear quadruply-stranded helicate/mesocate complexes. A detailed study of these supramolecular architectures has advanced our knowledge of the origins of magnetic relaxation in SMMs which was shown to arise from minute changes in bond distances around the metal centers leading to changes in the local anisotropy and, in turn, the effective energy barriers.

Introduction

Single-Molecule Magnets (SMMs) have been the focus of considerable research efforts due to their magnetic bi-stable properties below a certain temperature known as the blocking temperature.[1,2] Their characteristic slow relaxation of the magnetization arises from an appreciable spin ground state (S) and negative uni-axial magnetic anisotropy (D).[3] In combination, these two factors can potentially yield very high anisotropic energy barriers for the reversal of the magnetization (U). The energy barrier U is defined as $S^2|D|$ and $(S^2 - 1/4)|D|$ for integer and half integer spins, respectively. Therefore, theoretically it is advantageous to increase S in order to achieve high energy barriers. During the first wave of first-row transition metal SMMs,[4–7] high spin ground states have been achieved through the synthesis of clusters with high nuclearities such as Mn_{19}[3] and Mn_{25}[6] or through structural modifications using well-designed ligands.[8] However, in such systems the increase of the total spin values yielded a decrease in the anisotropy of the system as was seen in Mn_6 complexes where fine-tuning the employed oxime ligand afforded a switch from an antiferromagnetically coupled ($S = 4$) to a ferromagnetically coupled system ($S = 12$).[8] Through this concept a record barrier ($U_{eff} = 86$ K) for a transition metal complex was achieved yet the overall negative D parameter decreased from 2.00 K to 0.62 K while increasing the S.[9]

Therefore, in recent years other strategies have been explored to obtain high energy barriers without diminishing the anisotropy. As such, the use of metals with large orbital angular momenta such as 4d and 5d metals resulted in large magnetic anisotropy as demonstrated by Dunbar, Long and co-workers.[10,11] Furthermore, the search for metals with even higher magnetic anisotropy led to lanthanide/actinide metals and the second wave of SMMs.[12–16] Their unquenched orbital angular momentum is a consequence of their buried f electron shell. Lanthanide SMMs of varying nuclearities have exhibited record anisotropic energy barriers up to $U_{eff} = 528$ K.[17] Previous concerns regarding the inefficient magnetic coupling of lanthanide metals have been recently alleviated by Long and co-workers through the synthesis of $\{Dy_2\}$ and $\{Tb_2\}$ complexes bridged by dinitrogen radicals which exhibit high energy barriers of $U_{eff} = 180$ K and 327 K and blocking temperatures of 8.3 and 14 K, respectively.[18,19]

The shift from 3d to 4d/5d to 4f/5f metals has illustrated the need for complexes with higher anisotropy values in addition to high spin values. Contrary to controlling the spin values, controlling the anisotropy has proven to be extremely difficult.

[a]*Department of Chemistry, University of Ottawa, 10 Marie Curie, Ottawa, ON, K1N6N5, Canada. E-mail: m.murugesu@uottawa.ca; Fax: (+1) 613-562-5170; Tel: (+1) 613-562-5800 x2733*
[b]*Centre for Catalysis Research and Innovation, 30 Marie-Curie, Ottawa, ON, K1N6N5, Canada.*
[c]*Division of Quantum and Physical Chemistry and INPAC-Institute for Nanoscale Physics and Chemistry, Katholieke Universiteit Leuven, Celestijnenlaan, 200F, 3001, Belgium.*
[d]*Institut Néel, CNRS & Université J. Fourier, BP 166, 25 Avenue des Martyrs, 38042 Grenoble, France.*

† Electronic supplementary information (ESI) available: Experimental and crystallographic data, IR and NMR analyses, description of physical measurements and other magnetic data, *ab initio* calculation methods and other data. CCDC reference numbers 785130, 818518 and 818519. For ESI and crystallographic data in CIF or other electronic format see DOI: 10.1039/c2sc01029a

Parallel alignment of the magnetic anisotropy axes in transition metal ions can have an additive effect on total anisotropy of a system.[2] Therefore, aligning the anisotropy axes in a molecule can potentially yield even larger *D* values and hence much higher barriers for spin reversal. This challenging approach prompted the investigation of dinuclear helicate complexes where the helical twist provides a way of tuning the anisotropy axes on the metal centers and thereby modulating their orientations relative to one another. Moreover, this approach also provides two metal centers in a near identical coordination environment where subtle differences such as orientation of anisotropic axes or energies of the first excited Kramers doublets on Dy sites, yields different relaxation processes. Therefore, through simple modifications, ligands can be designed to modulate the angle between the anisotropic axes without changing the coordination environments such that correlations between the structural features and the magnetic properties can be studied. This strategy could lead to important magnetostructural correlations that enable us to synthesize SMMs with considerably larger barriers by controlling the magnetic anisotropy of the system as a whole.

Helical structures have been mainly dominated in the literature by single-,[20–22] double-[23–25] and triple-[26,27] stranded helicates. Only a few examples of quadruply-stranded helicates[28] have been reported to date where the synthetic strategy mainly focuses on employing metal ions with a square planar geometry and oligo-monodentate ligands acting as bridges. Only recently has there been reports of quadruply-stranded dinuclear helicates that were obtained using a different strategy.[29] The formulation involved oligobidentate bridging ligands and metal ions that can accommodate higher coordination numbers. Lanthanide helicates have also been investigated due to their ability to coordinate up to 12, but more commonly 8 or 9, donor atoms.[30] One of the key challenges in controlling the self-assembly of helicates has been to modulate the chiral amplification or helix reversal in these structures. As a result, a racemic mixture of homochiral complexes is observed where, in a dinuclear system, ΔΔ and ΛΛ symmetry is assigned. When an internal helix reversal occurs, it results in a ΛΔ *meso*-helical structure or mesocate and a loss of chirality. These achiral structures remain relatively unexplored.

Ligand design is key in the synthesis of helical architectures especially for the purpose of controlling the helical twist and thereby controlling the orientation of the anisotropic axes in the complex. A suitable ligand must possess at least two coordinating ends which are ideal for coordinating targeted metal ions. These moieties must be separated by a rigid spacer to prevent the thermodynamically driven chelate effect to encapsulate a single metal ion forming mononuclear complexes. The spacer must also provide some flexibility to allow for a helical twist of the ligand.[31] In pursuit of a deeper understanding of the self-assembly of helicates and mesocates as well as controlling the helical twist of the ligands we designed a strategy involving ligand modification to tune the length and flexibility of the spacer as seen in Fig. 1.

It is well known that N- and mostly O-based coordination environments favor the encapsulation of lanthanide ions.[32] It was therefore evident that maintaining the same coordinating pockets and metal ions should result in isomorphous complexes regardless of simple modifications to the spacer of the ligand. By varying only one parameter at a time, a correlation could be obtained between the properties of the spacer and the most thermodynamically stable structure. Furthermore, a series of compounds with varying spacers could be used as a model system for studying magnetostructural correlations leading to parameters which can be modified to obtain SMMs with higher energy barriers. Helical complexes provide a way to align the anisotropic axes of the molecules based on the degree of helical twist dictated by the ligands employed as seen in Fig. 1. To increase the length and flexibility of the spacer, systematic modifications included replacing the phenyl ring in *N*,*N*′-bi(3-methoxysalicylidene)benzene-1,4-diamine (H_2L^1) with a biphenyl group to yield *N*,*N*′-bi(3-methoxysalicylidene)biphenyl-4,4′-diamine (H_2L^2) as well as a diphenylmethane group yielding *N*,*N*′-bi(3-methoxysalicylidene)-4,4′-methylenedianiline (H_2L^3).

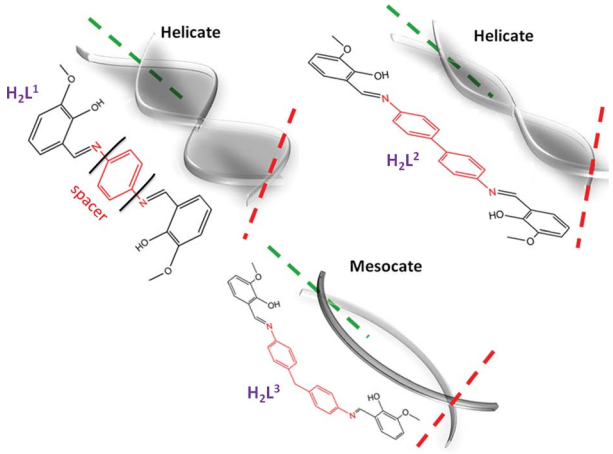

Fig. 1 Spacer modifications from H_2L^1 to H_2L^2 and H_2L^3 provide a way of controlling the relative orientation of the anisotropic axes on each metal center. Green and red dashed lines indicate anisotropic axes on Dy^{III} centers. *Vide infra* for anisotropic axes calculations.

Results and discussion

The reaction of $Dy(NO_3)_3 \cdot 6H_2O$ with the corresponding ligand in a 1 : 2 ratio and tetraethylammonium hydroxide (4 equiv.) in acetone/DMF (20 mL : 5 mL) (**1** and **3**) or DMF (**2**) affords yellow crystals. They are characterized as rare Dy^{III}_2 quadruply-stranded helicates $(NEt_4)_2[Dy_2(L^1)_4]((CH_3)_2CO)_{0.25}$ (**1**), $(NEt_4)_2[Dy_2(L^2)_4](H_2O)(DMF)_{0.5}$ (**2**) and mesocate $(NEt_4)_2[Dy_2(L^3)_4](Et_2O)_2((CH_3)_2CO)_{1.5}$ (**3**). The reaction requires basic conditions to promote the deprotonation of the ligand resulting in bridging anionic moieties. Single crystal X-ray analysis revealed dinuclear Dy^{III} helicate structures for **1** and **2** (Fig. 2a and 2b) and a mesocate structure for **3** (Fig. 2c). Complexes **1** and **3** crystallize in the monoclinic space group $P2_1/n$, whereas complex **2** crystallizes in the triclinic space group $P\bar{1}$. The helical and *meso*-helical structures are formed by four ligands intertwining around two crystallographically independent Dy^{III} metal centers. Since chirality in the case of **1** and **2** is generated from achiral entities, a racemic mixture of enantiomers is expected and indeed observed where both ΔΔ and ΛΛ isomers are present in the crystal packing.

The two Dy^{III} ions are eight-coordinate with coordination environments consisting of six oxygen and two nitrogen atoms. The ligands bind in an antiparallel fashion where one donor set

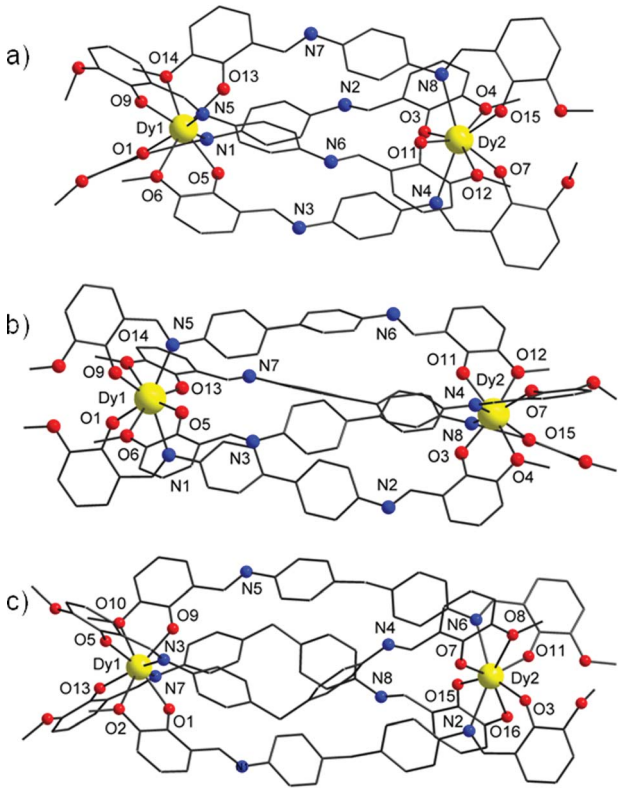

Fig. 2 Helicates $(NEt_4)_2[Dy_2(L^1)_4]((CH_3)_2CO)_{0.25}$ (**1**, a) $(NEt_4)_2[Dy_2(L^2)_4](H_2O)(DMF)_{0.5}$ (**2**, b) and mesocate $(NEt_4)_2[Dy_2(L^3)_4](Et_2O)_2((CH_3)_2CO)_{1.5}$ (**3**, c) are presented. Hydrogen atoms have been omitted for clarity. Color code: yellow (Dy), red (O), blue (N), grey (C).

consists of phenoxy and methoxy O atoms whereas the other donor set consists of phenoxy O and imino N atoms. The average Dy–N distances in **1**, **2** and **3** are 2.66, 2.63 and 2.64 Å, respectively. The average Dy–$O_{phenoxy}$ distance is 2.23 Å for **1** and **2** and 2.21 Å for **3** whereas the average Dy–$O_{methoxy}$ distances for **1**, **2** and **3** are 2.61, 2.62 and 2.60 Å, respectively. The coordination environment of each Dy^{III} center is slightly different in each complex with detailed bond distances presented in Table S1.† The two Dy^{III} ions are separated intramolecularly by 10.81 Å in **1**, 14.87 Å in **2** and 15.30 Å in **3**. By increasing the length of the spacer in the ligand, it is expected that the distance between the metal centers will increase as well as subtle differences in bond lengths will result around each metal center.

Previous studies involving triple-stranded helicates and linear alkyl bridging ligands have shown that the stereoselective formation of a helicate *versus* mesocate is a function of the number of methylene groups in the spacer.[33] An even number of methylene groups results in a chiral helicate whereas an odd number favors an achiral mesocate. Although this applies in most cases, in homochiral helicates **1** and **2**, there are no methylene groups in the spacer. There are, however, phenyl rings which maintain the rigidity of the ligand. This mechanical coupling between the lanthanide centers prevents the structure from adopting the zigzag conformation indicated by the odd number of methylene groups. Therefore, in a way the *odd–even* rule can still apply if the conformations are considered rather than the number of methylene groups. In mesocate **3**, there is one methylene group in the spacer favoring a bent conformation of the ligand yielding an internal mirror plane and a mesocate structure. Comparing all three complexes, a loss of helicity is evident in **3** (Fig. 3).

Magnetic susceptibility measurements were carried out for **1**, **2** and **3** in an applied dc field of 1000 Oe in the temperature range of 1.8–300 K (Fig. S1, ESI†). At room temperature, the χT values for **1**, **2** and **3** are 28.16, 28.10 and 28.08 $cm^3\ Kmol^{-1}$, respectively, which are in good agreement with the expected value of 28.34 $cm^3\ Kmol^{-1}$ for two uncoupled Dy^{III} ions ($S = 5/2$, $L = 5$, $^6H_{15/2}$, $g = 4/3$). The χT product remains relatively constant above 60 K before rapidly decreasing at lower temperatures reaching 23.25, 22.21 and 21.68 $cm^3\ Kmol^{-1}$ for **1**, **2** and **3**, respectively, at 2 K. This behavior is generally indicative of intramolecular antiferromagnetic coupling of the metal centers. However, due to a large physical separation between the Dy^{III} ions, this behavior most likely arises from the thermal depopulation of the Stark sub-levels and/or from the presence of large anisotropy in the system. The magnetization plots, *M vs. H*/*T*, for complexes **1**, **2** and **3** show field dependence of the magnetization that does not saturate at low temperatures (1.8 K for **1** and 1.9 K for **2** and **3**) and high magnetic fields (up to 7 T) (Fig. S2, ESI†) indicating the presence of significant magnetoanisotropy and/or low lying excited states in all three systems.

In order to investigate the possibility of SMM behavior, ac magnetic susceptibility measurements were carried out under zero dc field. The characteristic frequency dependence of the out-of-phase signal, χ'', below 14 K for **1** and 10 K for **2** and **3** indicates that all three complexes potentially behave as SMMs (Fig. S3–S5, ESI†). However, in that temperature range no maxima of χ'' are observed which can be attributed to small relaxation barriers resulting from quantum tunnelling of the magnetization (QTM) commonly observed in lanthanide systems.[34] Although the spin-parity effect indicates that QTM should not occur in half-integer spin systems, it is reasonable to speculate that this QTM is occurring between entangled states of nuclear and electronic spins which has been previously studied by

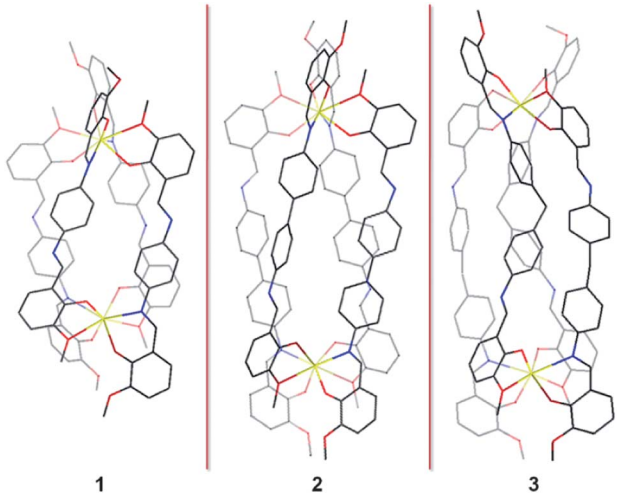

Fig. 3 The helical twist of the ligand around the metal centers in complexes **1** and **2** is evident whereas in complex **3**, the bending of the ligand results in a mesocate structure. Bold atoms are in front, faded atoms are in the back.

Ishikawa and Wernsdorfer in lanthanide SMMs.[35] In order to shortcut the QTM, ac measurements were carried out under an optimum dc field (the field at which the minimum of the characteristic frequency is observed, Fig. S6†) of 1600 Oe for **1** and **3** and 1200 Oe for **2** (Fig. 4, *left*) where the quantum tunnelling is minimized. Under the aforementioned applied dc fields, maxima are observed at 3.3 and 8.4 K for **1**, 7.4 K for **2** and 2.9 K for **3**, for 1500 Hz frequency. Two unique relaxation processes are observed for **1** (Fig. 4, *top*) whereas in **2** and **3** only one is evident (Fig. 4, *middle* and *bottom*, respectively) at the indicated temperature and frequency range. The thermally activated relaxation follows an Arrhenius-like behavior ($\tau = \tau_0 \exp(U_{\text{eff}}/kT)$) where the anisotropic energy barriers are calculated to be $U_{\text{eff}} = 13$ K ($\tau_0 = 1.92 \times 10^{-6}$ s) and $U_{\text{eff}} = 101$ K ($\tau_0 = 6.78 \times 10^{-10}$ s) for the low temperature and high temperature domains, respectively for **1**, 71 K ($\tau_0 = 5.93 \times 10^{-7}$ s) for **2** and 20 K ($\tau_0 = 1.45 \times 10^{-7}$ s) for **3** (Fig. 5). In order to further investigate relaxation mechanisms ac data as a function of frequency was collected in the 0.1–1500 Hz range. The variation of χ'' as a function of frequency for all three complexes further corroborates the presence of two clear maxima indicating two distinct relaxation processes for **1** and **3**, while for **2**, one peak with a slight shoulder is observed (Fig. S7, ESI†). The Cole–Cole plots[36] in the temperature range 2–8 K for **1** and **2**, as well as 2–4 K for **3** show multiple relaxation processes with a transition between fairly symmetric semi-circles at high temperature to unsymmetric curves for **1** (Fig. S8, ESI,† *top*). For the high temperature region (6–8 K), the data can be fitted using a generalized Debye model with a mean α parameter value of 0.32, indicating a moderate width of relaxation time for this temperature range. For **2**, the fit obtained (Fig. S8, ESI,† *middle*) yielded a mean α parameter value of 0.07 at high temperatures (6–8 K) and 0.31 at low temperature (2–3 K) indicating that the curves were becoming more unsymmetric. For **3**, no reasonable fit could be obtained clearly indicating the presence of more than one relaxation mode (Fig. S8, ESI,† *bottom*). To further investigate the observed secondary relaxation process at frequencies below 10 Hz for **3** (Fig. S7, ESI,† *left*), ac measurements were carried out in the 0.1 to 1500 Hz range under various static dc fields (0–8400 Oe) (Fig. S9, ESI†). The resulting χ'' *vs.* frequency curves were fitted using a convolution of two Casimir and Du Pré functions[37] (Fig. S10, ESI†) and the obtained relaxation times (τ_{slow} and τ_{fast}) are shown in Table S2.† At fields below 1000 Oe only the fast relaxation process is observed, whereas above 3600 Oe the faster process vanishes leaving only the slower process to dominate. The obtained data clearly indicate the importance of the magnitude of the applied static field in favoring different relaxation processes. The fraction of the susceptibility involved in the relaxation process can be assessed as the difference between isothermal and adiabatic susceptibility ($\chi_T - \chi_s$) *vs.* H for the slow and fast relaxation processes derived from fitting of the χ'' *vs.* frequency curves (Fig. S11, ESI†). Further studies at frequencies above 1500 Hz using a PPMS magnetometer might reveal other relaxation processes for all complexes; these studies will be reported in the near future.

The ac data indicates that relaxation processes are significantly affected by very subtle changes in the coordination environments around the metal centers.[38] Given that the anisotropy barrier in 4f single-ion systems could be directly related to the sub-level

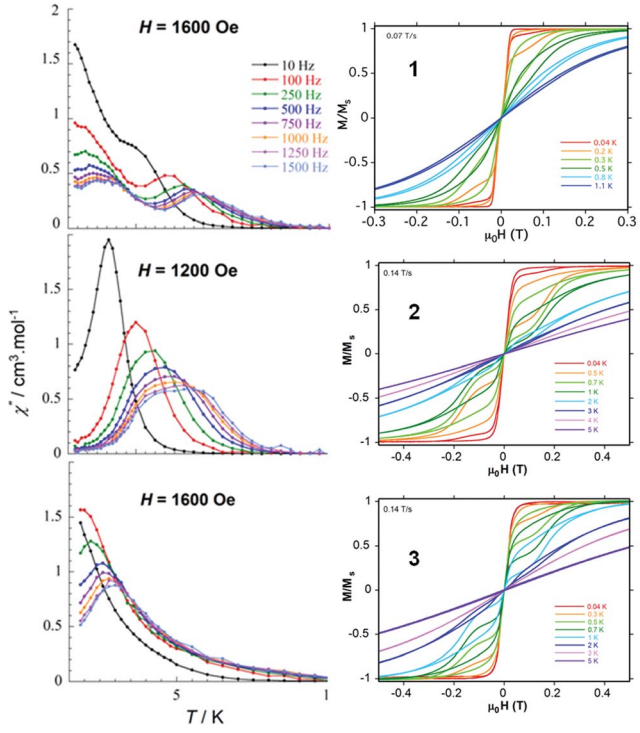

Fig. 4 *Left*: Temperature dependence of the out-of-phase magnetic susceptibility, χ'', for **1** (*top*), **2** (*middle*) and **3** (*bottom*) in applied optimum fields of 1600 Oe, 1200 Oe and 1600 Oe, respectively. *Right*: Magnetization (M) *vs.* applied dc field sweeps at the indicated sweep rate and temperatures. M is normalized to its saturation value, M_s, at 0.3 T for **1** (*top*), **2** (*middle*) and **3** (*bottom*).

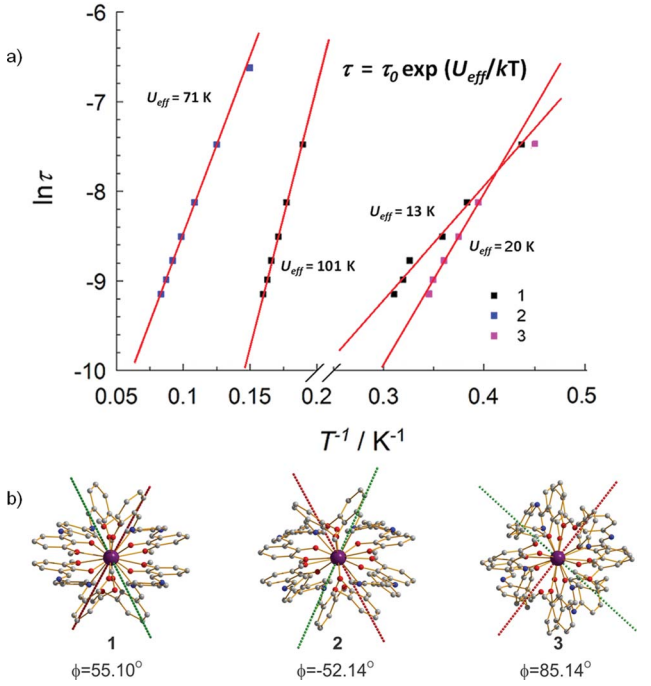

Fig. 5 a) The relaxation time is plotted as $\ln(\tau)$ *vs.* T^{-1} for complexes **1–3**. b) Comparison of the angle (ϕ) between the anisotropy axes of both Dy ions for all three complexes.

structure of the ground state multiplets (which results from ligand field effects), it is of critical importance to determine the exact geometry of the coordination polyhedron.[39] This can be carried out using *Shape* software.[40] The results reveal that both Dy^{III} ions in each complex adopt an intermediate geometry between a square antiprism (D_{4d}) and a dodecahedron (D_{2d}). However, subtle but significant differences in the coordination geometry appear between the two Dy^{III} ions which alter the sublevel structures and therefore lead to two distinct relaxation processes. Across all three complexes, coordination environments of Dy^{III} ions seem almost identical to the naked eye; however, slight differences in bond lengths (Table S1, ESI†) are shown to drastically affect the SMM properties. In order to further probe the low temperature behavior, single crystal dc relaxation measurements were performed on a micro-SQUID[41] in the temperature range 5.0–0.04 K (Fig. 4, *right*). It is noteworthy that the loops at zero field are negligible. This is mainly due to the fast tunnelling effect taking place at zero field. When a field is applied, an opening of a hysteresis loop can be observed below 1.1 K for **1** and 5 K for **2** and **3**. The coercivity increases with decreasing temperature (and increasing sweep rates as seen in Fig. S12, ESI†) indicating field-induced SMM-like behavior due to switching off of the QTM under an applied field. Additionally the hysteresis loops indicate an exchange-biased system with weak exchange coupling corresponding to 11.5 mT (**1**), 13 mT (**2**) and 18 mT (**3**) determined through low temperature dc measurements. These dipole interactions could arise from intra- as well as intermolecular interactions. This behavior thus confirms the appearance of frequency dependant out-of-phase signals in the ac data (Fig. 4, *left*).

In order to further investigate and confirm the observed magnetic behavior, *ab initio* calculations of CASSCF/RASSI/SINGLE_ANISO type[42,43] have been performed on the individual dysprosium fragments for all complexes (Fig. S13, Tables S3–S5, ESI†). The obtained energies of the lowest Kramers doublets on each Dy ion in complexes **1–3** are listed in Table 1. Due to large distances between dysprosium ions in each molecule, the intramolecular exchange interaction is negligible and the interaction between magnetic ions mainly originates from their dipolar interactions. The latter interactions are also weak (Table 1) compared to the temperature of ac measurements, therefore, the blockage of the reversal of the magnetization arises mainly from individual dysprosium ions as was also seen in other polynuclear Dy complexes.[16] The spectrum of the lowest exchange multiplets in **1–3** is given in Table S6† and the calculated magnetic properties are shown in Fig. S14–S17.†

The calculated energies of the first excited Kramers doublets on two Dy sites (Table 1) differ significantly for **1** thus explaining the presence of two distinct Orbach relaxation times in this complex (Fig. 5a). Moreover, the excitation energies (84.67 cm^{-1} and 35.94 cm^{-1}) are in reasonable agreement with the two energy barriers extracted from the experiment (101 K and 13 K). The remaining discrepancy can be explained by two reasons. First, the values of the energy barriers extracted from the data on Fig. 5a are quite sensitive to the chosen experimental points through which the straight line is drawn. For example, by not taking into account the three last points for the lower barrier of **1**, the resulting straight line will be twice steeper and the blocking barrier twice larger compared to 13 K derived in Fig. 5a. Second, the accuracy of present *ab initio* calculations, which were limited to a CASSCF level, probably are in the range of one of several tens of wavenumbers. Indeed, shifting slightly the energies of the first excited Kramers doublets on Dy sites (Table S7, ESI†), which would imply the energies of the barriers of 28.5 cm^{-1} and 72 cm^{-1}, respectively, reproduces very well the χT curve and improves significantly the $M(H)$ dependencies (Fig. S18 and S19, ESI†).

Table 1 Energies of the lowest eight Kramers doublets on Dy^{III} sites (cm^{-1}), the main components of the *g* tensor for the ground Kramers doublets and the angle between the main magnetic axes on the dysprosium sites are presented

1		**2**		**3**	
Dy1	Dy2	Dy1	Dy2	Dy1	Dy2
0.00	0.00	0.00	0.00	0.00	0.00
84.67	35.94	32.00	33.17	35.21	23.18
188.38	174.76	128.35	149.26	150.66	151.51
261.40	224.61	172.36	162.89	188.21	204.62
280.27	255.67	217.69	231.91	284.40	315.61
339.64	333.95	295.74	318.14	378.08	420.86
381.06	373.01	409.28	395.24	461.11	486.75
575.63	570.38	475.85	523.65	553.62	634.13
		g factors for the ground Kramers doublets			
0.0312	0.0873	0.0701	0.1874	0.1342	0.0835
0.0403	0.2060	0.1462	0.3934	0.3842	0.4177
19.6312	18.8964	18.1150	17.6409	17.4299	15.9935
		Angle between main magnetic axes (°)			
55.10		52.14		85.14	
		Dipolar intramolecular coupling[a] (cm^{-1}) and the corresponding tunneling splittings of the first exchange doublet (cm^{-1})			
J_{dip}	Δ_{tun}	J_{dip}	Δ_{tun}	J_{dip}	Δ_{tun}
−0.146	1.2×10^{-6}	-2.4×10^{-3}	4.7×10^{-5}	-2.8×10^{-3}	1.6×10^{-5}

[a] J_{dip} enter the following Hamiltonian: $H = -J_{dip}\tilde{S}_1 \cdot \tilde{S}_2$, where $\tilde{S}_i$ are pseudospins $s = ½$ of the ground Kramers doublets on Dy sites.

On the other hand, the energies of the first excited Kramers doublets on two dysprosium sites in **2** and **3** do not differ much, which is in accordance with close values of relaxation times in each of these compounds (Fig. 5a). For **2**, the calculated energies of the first excited states on Dy sites seems to be slightly underestimated, while a small upshift (Table S7, ESI†) makes them close to the extracted barrier in Fig. 5a and improves significantly the $M(H)$ dependencies (Fig. S20, ESI†). At the same time the experimental points corresponding to **3** in Fig. 5a still bend down in the high-T region, which means that the Arrhenius regime should show up at still higher temperatures. Taking the first points only will give a much steeper line and a higher barrier. Accordingly, the calculated energies of the first excited Kramers doublets should be upshifted (Table S7, ESI†), which also improves the calculated $M(H)$ dependencies (Fig. S21, ESI†).

The calculations for all three compounds give relatively large transversal components (g_x and g_y) of the g tensors for the ground Kramers doublets on the dysprosium sites compared to other complexes.[44] This implies relatively high relaxation rates in the tunnelling (quantum) regime, which are also revealed in the fact that the blocking of magnetization is detected in ac susceptibility only under applied dc field. As a result, the thermally activated regime is observed at temperatures where the relaxation rates are high, *i.e.* τ is small (Fig. 5a). At the same time the intramolecular dipolar interaction does not contribute to the blocking of magnetization at the investigated temperatures, being of the order of intermolecular dipolar interaction (Table 1).

The data clearly indicates a correlation between the ligand field and the energies of the excited states of each Dy^{III} ion and hence the magnetic properties of the complexes. Observing one or more relaxation processes in the out-of-phase plots can not only be associated with the number of crystallographically independent metal ions but more specifically with the associated energies of the excited states as evident from this system. *Ab initio* calculations were performed to determine the orientation of the anisotropic axes on each Dy^{III} center (Fig. 5b). The observed angles of 55.10° (**1**), 52.14° (**2**) and 85.14° (**3**) between the anisotropic axes are shown to vary depending on the spacer used in the ligand. This data clearly indicates that it is possible to control the orientation of the axes by controlling the helical twist encoded in the ligand.

Conclusion

The synthetic strategy employed above proved successful in predicting the helicity for rare, quadruply-stranded lanthanide complexes. Complexes **1**, **2** and **3** are part of a series of compounds synthesized for the purpose of studying the orientation of the anisotropic axes of lanthanide metal centers as a function of the helical twist dictated by the ligand. As the length and flexibility of the ligand is varied, the angle between the axes varies as well. These results confirm that, in fact, it is possible to control the magnetic axes relative to one another by simply modifying the spacer of the ligand which will allow us to synthesize SMMs with potentially higher anisotropic energy barriers. By exploring supramolecular architectures for the purpose of controlling the anisotropy in a complex, we have shown that it is possible to rationally design and synthesize SMMs using ligands which dictate specific structural motifs. All three complexes exhibit field-induced SMM behavior and are thus the first quadruply-stranded lanthanide helicates and mesocate SMMs reported to date. Additionally, caution should be taken when analysing magnetic susceptibility data; all three complexes exhibit varying relaxation processes which were difficult to explain initially. However, we were able to show that they arise from very subtle changes in the coordination environments of each metal center which was further confirmed by *ab initio* calculations showing different excitation energies for both metal centers in each complex. It is noteworthy that subtle differences in coordination environments leading to drastic changes in orientation of the anisotropic axis was reported by Sessoli and co-workers for a mononuclear system.[45] However, we have shown that minute differences in bond lengths around each Dy^{III} center result in clear changes to the local anisotropy which has never been previously reported for a dinuclear system. Although the magnetic behavior was shown to mainly arise from changes to the local coordination sphere of each Dy^{III} ion rather than the alignment of anisotropic axes in the complex, this system demonstrates clear proof-of-principle that the angle between the axes can be controlled. The limitations of the system, however, involving the distance between the metal centers can be overcome. We are currently investigating the use of shorter bridging ligands as well as using radical bridges while maintaining the helical arrangements to induce magnetic coupling between Dy^{III} ions. Finally, controlling the molecular architecture of novel magnetic systems will not only shed some light on their unique magnetic behavior but will also pave the way forward towards the design and isolation of functional molecular materials.

Acknowledgements

We thank the University of Ottawa, CCRI, NSERC (Discovery and RTI grants); ERA, Vision 2010, CFI, ORF, FFCR. L. Ungur is a postdoctoral researcher of the FWO-Vlanderen (Fonds Wetenschappelijk Onderzoek). Financial support of the Methusalem program of the K.U. Leuven is gratefully acknowledged.

Notes and references

1 R. Sessoli, D. Gatteschi, A. Caneschi and M. A. Novak, *Nature*, 1993, **365**, 141.
2 R. Sessoli, H.-L. Tsai, A. R. Schake, S. Wang, J. B. Vincent, K. Folting, D. Gatteschi, G. Christou and D. N. Hendrickson, *J. Am. Chem. Soc.*, 1993, **115**, 1804.
3 G. Christou, D. Gatteschi, D. N. Hendrickson and R. Sessoli, *MRS Bull.*, 2000, **25**, 66.
4 C. M. Zaleski, E. C. Depperman, J. W. Kampf, M. L. Kirk and V. L. Pecoraro, *Angew. Chem., Int. Ed.*, 2004, **43**, 3912.
5 M. Soler, W. Wernsdorfer, K. Folting, M. Pink and G. Christou, *J. Am. Chem. Soc.*, 2004, **126**, 2156.
6 M. Murugesu, M. Habrych, W. Wernsdorfer, K. A. Abboud and G. Christou, *J. Am. Chem. Soc.*, 2004, **126**, 4766.
7 A. M. Ako, I. J. Hewitt, V. Mereacre, R. Clérac, W. Wernsdorfer, C. E. Anson and A. K. Powell, *Angew. Chem., Int. Ed.*, 2006, **45**, 4926.
8 C. J. Milios, A. Vinslava, W. Wemsdorfer, S. Moggach, S. Parsons, S. P. Perlepes, G. Christou and E. K. Brechin, *J. Am. Chem. Soc.*, 2007, **129**, 2754.
9 C. J. Milios, S. Piligkos and E. K. Brechin, *Dalton Trans.*, 2008, 1809.
10 E. J. Schelter, A. V. Prosvirin and K. R. Dunbar, *J. Am. Chem. Soc.*, 2004, **126**, 15004.
11 D. E. Freedman, D. M. Jenkins, A. T. DIavarone and J. R. Long, *J. Am. Chem. Soc.*, 2008, **130**, 2884.

12 P.-H. Lin, T. J. Burchell, R. Clérac and M. Murugesu, *Angew. Chem., Int. Ed.*, 2008, **47**, 8980.
13 N. Ishikawa, M. Sugita, T. Ishikawa, S.-Y. Koshihara and Y. Kaizu, *J. Am. Chem. Soc.*, 2003, **125**, 8694.
14 J. Tang, I. Hewitt, N. T. Madhu, G. Chastanet, W. Wernsdorfer, C. E. Anson, C. Benelli, R. Sessoli and A. K. Powell, *Angew. Chem., Int. Ed.*, 2006, **45**, 1729.
15 D. P. Mills, F. Moro, J. McMaster, J. van Slageren, W. Lewis, A. J. Blake and S. T. Liddle, *Nat. Chem.*, 2011, **3**, 454.
16 P.-H. Lin, T. J. Burchell, L. Ungur, L. F. Chibotaru, W. Wernsdorfer and M. Murugesu, *Angew. Chem., Int. Ed.*, 2009, **48**, 9489.
17 R. J. Blagg, C. A. Muryn, E. J. L. McInnes, F. Tuna and R. E. P. Winpenny, *Angew. Chem., Int. Ed.*, 2011, **50**, 6530.
18 J. D. Rinehart, M. Fang, W. J. Evans and J. R. Long, *Nat. Chem.*, 2011, **3**, 538.
19 J. D. Rinehart, M. Fang, W. J. Evans and J. R. Long, *J. Am. Chem. Soc.*, 2011, **133**, 14236.
20 C. J. Cathey, E. C. Constable, M. J. Hannon, D. A. Tocher and M. D. Ward, *J. Chem. Soc., Chem. Commun.*, 1990, 621.
21 R. P. Thummel, C. Hery, D. Williamson and F. Lefoulon, *J. Am. Chem. Soc.*, 1988, **110**, 7894.
22 N. K. Al-Rasbi, H. Adams, L. P. Harding and M. D. Ward, *Eur. J. Inorg. Chem.*, 2007, **2007**, 4770.
23 E. A. Medlycott and G. S. Hanan, *Chem. Commun.*, 2007, 4884.
24 K. Miwa, Y. Furusho and E. Yashima, *Nat. Chem.*, 2010, **2**, 444.
25 V. E. Campbell, X. de Hatten, N. Delsuc, B. Kauffmann, I. Huc and J. R. Nitschke, *Nat. Chem.*, 2010, **2**, 684.
26 J.-J. Jiang, S.-R. Zheng, Y. Liu, M. Pan, W. Wang and C.-Y. Su, *Inorg. Chem.*, 2008, **47**, 10692.
27 K. Zeckert, J. Hamacek, J.-M. Senegas, N. Dalla-Favera, S. Floquet, G. Bernardinelli and C. Piguet, *Angew. Chem., Int. Ed.*, 2005, **44**, 7954.
28 J. Xu and K. N. Raymond, *Angew. Chem., Int. Ed.*, 2006, **45**, 6480.
29 A. P. Bassett, S. W. Magennis, P. B. Glover, D. J. Lewis, N. Spencer, S. Parsons, R. M. Williams, L. De Cola and Z. Pikramenou, *J. Am. Chem. Soc.*, 2004, **126**, 9413.
30 J. Inanaga, H. Furuno and T. Hayano, *Chem. Rev.*, 2002, **102**, 2211.
31 G. F. Swiegers and T. J. Malefetse, *Chem. Rev.*, 2000, **100**, 3483.
32 I. Hewitt, J. Tang, N. T. Madhu, C. E. Anson, Y. Lan, J. Luzon, M. Etienne, R. Sessoli and A. K. Powell, *Angew. Chem., Int. Ed.*, 2010, **49**, 6352.
33 M. Albrecht, I. Janser, H. Houjou and R. Frohlich, *Chem.–Eur. J.*, 2004, **10**, 2839.
34 J. Long, F. Habib, P.-H. Lin, I. Korobkov, G. Enright, L. Ungur, W. Wernsdorfer, L. F. Chibotaru and Muralee Murugesu, *J. Am. Chem. Soc.*, 2011, **133**, 5319.
35 N. Ishikawa, M. Sugita and W. Wernsdorfer, *Angew. Chem., Int. Ed.*, 2005, **44**, 2931.
36 (*a*) K. S. Cole and R. H. Cole, *J. Chem. Soc.*, 1941, **9**, 341; (*b*) S. M. J. Aubin, Z. Sun, L. Pardi, J. Krzystek, K. Folting, L. J. Brunel, A. L. Rheingold, G. Christou and D. N. Hendrickson, *Inorg. Chem.*, 1999, **38**, 5329.
37 P.-E. Car, M. Perfetti, M. Mannini, A. Favre, A. Caneschi and R. Sessoli, *Chem. Commun.*, 2011, **47**, 3751 and references therein.
38 L. Sorace, C. Benelli and D. Gatteschi, *Chem. Soc. Rev.*, 2011, **40**, 3092.
39 N. Ishikawa, Y. Mizuno, S. Takamatsu, T. Ishikawa and S.-Y. Koshihara, *Inorg. Chem.*, 2008, **47**, 10217.
40 D. Casanova, M. Llunel, P. Alemany and S. Alvarez, *Chem.–Eur. J.*, 2005, **11**, 1479.
41 W. Wernsdorfer, *Supercond. Sci. Technol.*, 2009, **22**, 064013.
42 F. Aquilante, L. De Vico, N. Ferre, G. Ghigo, P.-Å. Malmqvist, P. Neograd, T. B. Pedersen, M. Pitonak, M. Reiher, B. O. Roos, L. Serrano-Andres, M. Urban, V. Veryazov and R. Lindh, *J. Comput. Chem.*, 2010, **31**, 224.
43 L. Ungur, W. Van den Heuvel and L. F. Chibotaru, *New J. Chem.*, 2009, **33**, 1224.
44 R. Sessoli and A. K. Powell, *Coord. Chem. Rev.*, 2009, **253**, 2328.
45 G. Cucinotta, M. Perfetti, J. Luzon, M. Etienne, P.-E. Car, A. Caneschi, G. Calvez, K. Bernot and R. Sessoli, *Angew. Chem., Int. Ed.*, 2012, **51**, 1606.

